

Correlations and hyperuniformity in the avalanche size of the Oslo Model

Rosalba Garcia-Millan,^{1,*} Gunnar Pruessner,¹ Luke Pickering,² and Kim Christensen²

¹*Department of Mathematics, Imperial College London,
180 Queen's Gate, London SW7 2BZ, United Kingdom*

²*The Blackett Laboratory, Imperial College London, London SW7 2BW, United Kingdom*

(Dated: October 3, 2017)

Hyperuniformity is a feature of some processes where correlations suppress fluctuations. Using a map to an interface picture we prove that a sequence of avalanche sizes of the Oslo Model are hyperuniform on long macroscopic timescales $M \gg M^*$ and Poisson-like on short timescales $M \ll M^*$, where the crossover point $M^* = L^{D(\tau-1)}$ is determined by the characteristic vertical fluctuations of the interfaces. Our results imply that, counterintuitively, more precise estimates of the moments of the avalanche size are obtained if the samples are correlated rather than if the samples are independent, implying a reduction of computing time for reliable estimates. We further show that when the driving site is chosen at random, the dominance of the drive noise over the interface noise prevents hyperuniformity. We support our findings with numerical results.

I. INTRODUCTION

The Oslo rice pile Model [1] has been extensively studied in the literature as a paradigmatic example of a non-equilibrium system that evolves spontaneously into a scale-invariant state thus considered a representative case of Self-Organised Criticality [1–7]. Due to the nature of the model, the successive avalanches in the pile are correlated. The quantities characterising the avalanche (e.g. size, extension and duration) depend to a large extent on the configuration of the pile. At the same time, during the relaxation process, the avalanche modifies the pile, leaving behind a different configuration to be explored by the next avalanche. However, because of the complexity of the model and the number of random variables involved, surprisingly little is understood about its correlations [4].

In particular, when supposed asymptotics of moments are studied, often probability density functions are sampled by deliberately generating effectively independent samples [8], for example by taking measurements once every so many relaxations in the pile. In this paper, we study the correlations of the avalanche size s in the Oslo Model and we show that more precise estimates are obtained when sampling sequentially than when sampling independently. Counterintuitively, the correlations within the pile suppress the fluctuations of the observables in amplitude and, in some cases, even in rate of convergence.

The study of temporal correlations between avalanches is a first step towards the understanding of predictability. For that reason, over the last decades it has been a very active subject of study not only in avalanche models such as the random-field Ising model [9], sandpile-like models [10] or driven interface depinning models [11], but also in a broad area of experiments, for example in neuroscience [12, 13], seismology [14, 15], sandpile-like experiments

[16], crackling noise signals [17], to name just a few.

In a time series of events X_t , $t \in \mathbb{N}$, its fluctuations may be characterised by the variance

$$\sigma^2(S(T)) \equiv \langle (S(T))^2 \rangle - \langle S(T) \rangle^2 \propto T^\lambda, \quad (1)$$

where $S(T) = X_1 + \dots + X_T$ and $\langle \bullet \rangle$ denotes an expectation. If X_t are identically distributed, the Central Limit Theorem [18] states that, in the absence of correlations, the variance grows proportionally to the sample size T , i.e. $\lambda = 1$. In the general case, for correlated random variables, calculating the variance in closed form can be very difficult if not impossible [19–21]. Interestingly, in some stochastic processes [22] and one-dimensional point patterns [23, 24], it has been proved that the negative correlations suppress fluctuations in such a way that $\lambda \in [0, 1)$. Such processes are called hyperuniform [23, 24], or, ingeniously translated, superhomogeneous [25]. A time series can be understood as a discrete one-dimensional case of a disordered d -dimensional point process, where the fluctuations are characterised by the variance of the number of particles in a volume [23]. Disordered hyperuniform systems suppress density fluctuations on large length scales, manifesting a regularity that is not apparent on short length scales. These anomalously small fluctuations have been studied in a wide range of contexts such as point patterns [23, 24, 26, 27], cosmology [25], jammed particle packings [28] and photonic band-gap materials [29].

We denote the estimator of the expectation $\langle X \rangle$ by an overbar \bar{X} , and define it as

$$\bar{X} = \frac{1}{T} \sum_{t=1}^T X_t = \frac{S(T)}{T}. \quad (2)$$

It is clear that the estimator is unbiased [30] since $\langle \bar{X} \rangle = \langle X \rangle$. From Eq. (1), the fluctuations of the estimator \bar{X} read

$$\sigma^2(\bar{X}(T)) = \frac{1}{T^2} \sigma^2(S(T)) \propto T^{\lambda-2}, \quad (3)$$

* Email address: garciamillan16@imperial.ac.uk

which implies that, if X is hyperuniform, then the rate of convergence of the estimator \bar{X} is faster than otherwise. In particular, if $\lambda = 0$, the rate of convergence is quadratic.

In the following we show that the temporal correlations in the avalanche size s in the Oslo Model reduce the fluctuations in the estimates \bar{s}^n of the moments $\langle s^n \rangle$. We will provide a proof for the hyperuniformity of s for the one-dimensional boundary driven Oslo Model. In addition, we complement our analytical findings with numerical results for a number of variants of the model, including two dimensions and external drive uniformly distributed on the lattice. In our numerical simulations, we compute the variance $\sigma^2(\bar{s}^n(T))$ from a sample of independent estimates $\{s_1^n(T), \dots, s_N^n(T)\}$ of \bar{s}^n , where each $s_i^n(T)$ is obtained from a window of observation of length $T \in \mathbb{N}$.

The remainder of this manuscript is organised as follows. In Section II we describe the original Oslo Model and its observables. In Section III we present an equivalent description by means of an interface interpretation and the governing stochastic equation of motion [2, 3]. In Sections IV and V we define and study the scaling laws of the avalanche size s and the multiple drive avalanche size $S(M; L)$ respectively. In Section VI we derive the scaling law of the fluctuations of the estimate of the first moment \bar{s} and compare these results with the fluctuations of higher moments and variations of the model, specifically allowing for bulk drive (uniformly distributed on the lattice), on both a one-dimensional and a two-dimensional pile.

II. THE OSLO MODEL

The Oslo Model was inspired by the experiment of a one-dimensional ricepile confined between two glass plates closed at one side and at the bottom [1]. Grains of rice were dropped at regular time intervals next to the closed boundary causing avalanches in the pile. Eventually, the pile spilled out the grains through the open boundary.

In the stochastic model, the rice pile sits on a one-dimensional lattice of size L and its configuration is described by the set of local slopes $z_x = n_x - n_{x+1}$, $x \in \{1, \dots, L\}$, where n_x is the number of grains and thus the height at x with boundary condition $n_{L+1} \equiv 0$. Each site has associated with it a randomly chosen critical slope $z_x^c \in \{1, 2\}$. Given $z_x \leq z_x^c$ for all $x \in \{1, \dots, L\}$, which is called a stable or quiescent configuration, the evolution of the pile follows the steps (i) *drive*, a grain is dropped at site $x = 1$ which results in $z_1 \rightarrow z_1 + 1$ (equivalently $n_1 \rightarrow n_1 + 1$); (ii) *relaxation*, every site $x \in \{1, \dots, L\}$ with $z_x > z_x^c$ is said to be unstable and is relaxed in parallel with all other unstable sites by toppling one grain to the neighbouring site on its right, resulting in the update rules $z_x \rightarrow z_x - 2$, $z_{x\pm 1} \rightarrow z_{x\pm 1} + 1$ in the bulk (equivalently $n_x \rightarrow n_x - 1$, $n_{x+1} \rightarrow n_{x+1} + 1$), and z_x^c redrawn afterwards to be either 1 or 2 with equal

probability. The relaxation process is repeated until the entire pile is in a stable configuration, also called quiescent state. The update rules that apply to the boundaries are $z_1 \rightarrow z_1 - 2$, $z_2 \rightarrow z_2 + 1$ (equivalently $n_1 \rightarrow n_1 - 1$, $n_2 \rightarrow n_2 + 1$) and $z_L \rightarrow z_L - 1$, $z_{L-1} \rightarrow z_{L-1} + 1$ (equivalently $n_L \rightarrow n_L - 1$). The number of slope units in the system is conserved during relaxation in the bulk but not at the boundary at $x = 1$, where slope units are lost at relaxation. We distinguish between the macroscopic timescale denoted by integer t , where the pile evolves from one stable configuration to another as t increases by 1, and a microscopic timescale on which the avalanches unfold. The microscopic timescale is infinitely separated from the macroscopic timescale and, measured on the macroscopic timescale, proceeds in steps of $\delta t \ll 1$ per sweep of parallel updates.

The parallel update introduced above is relevant only as far as the equation of motion in Section III is concerned. Otherwise the model is Abelian [7] so that final states reached after any avalanche are independent of the order of updates. Variations of the model that we have studied in this paper include changing the boundary conditions, extending the model to two dimensions and allowing the drive to occur uniformly across the lattice.

III. THE INTERFACE PICTURE

The dynamics of the pile can be equivalently described by means of a stochastic equation of motion and the corresponding initial and boundary conditions [3]. For simplicity, suppose the pile initially is in the state $z_x = 1$ for all $x \in \{1, \dots, L\}$. Let $h(x, t)$ be the number of slope unit charges at site x up to time $t \geq 0$, and let $\eta(x, h(x, t))$ be a quenched noise that takes values 0 if $h(x, t)$ is even, and 1 or -1 with equal probability if $h(x, t)$ is odd.

The random variable η is quenched in the sense that it is allowed to change value only if the argument h changes value after an update. For this reason, η is a function of x and $h(x, t)$, but not t . However, to ease the notation, we write

$$\eta_{x,t} \equiv \eta(x, h(x, t)), \quad (4)$$

as for each x and t there is a unique value of $h(x, t)$. The stable configuration of the pile is encoded in η via the relation $\eta_{x,t} = 1 - z_x$. Given that $\{z_x\}$ is Markovian by definition of the model, it is clear that η is Markovian as well.

The microscopic temporal evolution of $h(x, t)$ for $x \in \{1, \dots, L\}$ is [3]

$$h(x, t + \delta t) - h(x, t) = \frac{1}{2} (h(x-1, t) - 2h(x, t) + h(x+1, t) + \eta_{x-1,t} + \eta_{x+1,t}). \quad (5)$$

This is an equation of motion; the evolution of the pile stops as soon as the right hand side of Eq. (5) vanishes and the quiescent configuration is then given by

$z_x = 1 - \eta_{x,t}$. The boundary conditions that reproduce the original Oslo Model are: open on the left with an external source $h(0,t) = 2E(t)$, where $E(t) = \lfloor t \rfloor \in \mathbb{N}$ is the drive; and closed on the right $h(L,t) = h(L+1,t)$. For convenience, we choose $\delta t \ll 1$ so that the number of microscopic time step updates in Eq. (5) of any individual avalanche is small compared to $1/\delta t$ so that driving takes place only when the configuration is stable. We make this choice so that time is measured in units of the number of grains added and all integer t indicate times of quiescence, which give the $h(x,t)$ we are interested in. Choosing the initial condition $h(x,0) = 0$ for all x means that the pile is stable initially, commensurate with $z_x = 1$. It is easily generalised later. These initial and boundary conditions need to be extended to η according to its updating rules, i.e. $\eta_{x,0} = 0$, $\eta_{0,t} = 0$ and $\eta_{L,t} = \eta_{L+1,t}$ for all x and t .

When the pile is in a quiescent state, the left-hand side of Eq. (5) vanishes for all x , giving the expression that governs the function $h(x,t)$ for $t \in \mathbb{N}$

$$\Delta h(x,t) = -a_{x,t}, \quad (6)$$

where $\Delta h(x,t)$ denotes the discrete Laplacian and $a_{x,t} = \eta_{x-1,t} + \eta_{x+1,t}$. The solution to Eq. (6) along with the initial and boundary conditions is

$$h(x,t) = 2E(t) + \sum_{i=1}^x i a_{i,t} + x \sum_{i=x+1}^L a_{i,t}. \quad (7)$$

In computer simulations of the Oslo Model it is observed that $\langle \eta \rangle_q < 0$ in a recurrent state at quiescence, which implies that the solution of $h(x,t)$ given in Eq. (7) has finite curvature.

For an arbitrary stable initial condition of the pile $\{z_x\}$, equivalently $\{\eta_{x,0}\}$, the equation of motion in (5) has the additional term $-(\eta_{x-1,0} + \eta_{x+1,0})/2$ on its right-hand side, thus Eq. (6) reads

$$\Delta h(x,t) = a_{x,0} - a_{x,t}, \quad (8)$$

and its solution is

$$h(x,t) = 2E(t) - \tilde{h}(x,0) + \sum_{i=1}^x i a_{i,t} + x \sum_{i=x+1}^L a_{i,t}, \quad (9)$$

where $\tilde{h}(x,0) = \sum_{i=1}^x i a_{i,0} + x \sum_{i=x+1}^L a_{i,0}$. The shift in $h(x,t)$ provided by $\tilde{h}(x,0)$ does not mean that the pile has long-term memory, as $h(x,t)$ is just a quantity integrated over time and \tilde{h} is an offset that accounts for the initial $\{z_x\}$. Henceforth, we will assume that the pile is initially at state $z_x = 1$, $x \in \{1, \dots, L\}$, so that $\tilde{h}(x,0) = 0$, without loss of generality.

The function $H(x,t)$ gives the total number of topplings at site x up to time t . In [3] it is shown that

$$H(x,t) = \frac{1}{2}(h(x,t) + \eta_{x,t}). \quad (10)$$

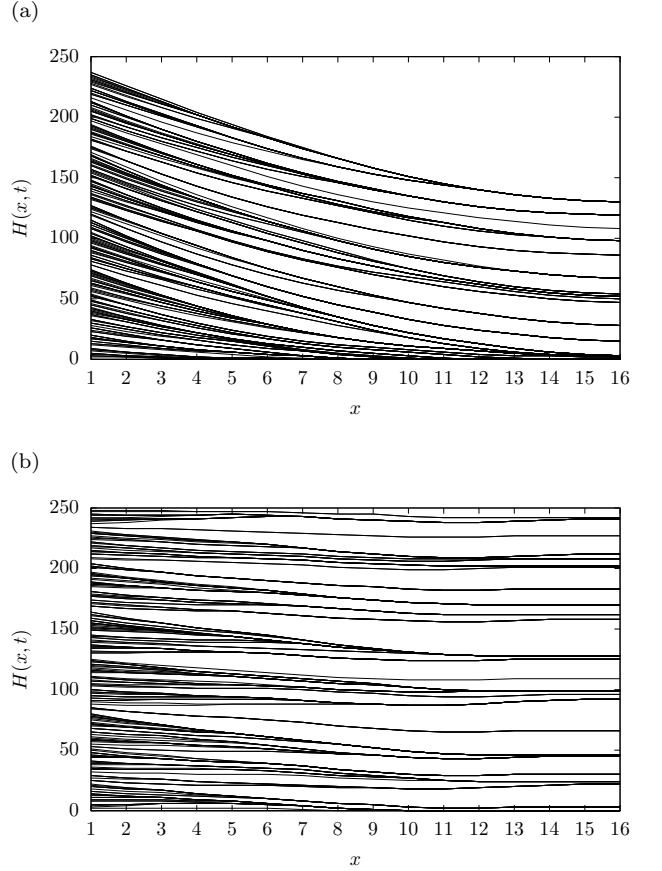


FIG. 1. Examples of the interface picture of the number of topplings $H(x,t)$ on a one-dimensional boundary-driven pile of size $L = 16$. The total drive size is 250 grains. In (a) the initial state of the pile is $z_x = 1$ and z_x^c chosen at random for all x and in (b) the initial state is the configuration of the pile after driving 1000 times the pile with $z_x = 1$ and random initial z_x^c .

Note that using the boundary conditions of h and η at $x = L$, the function $H(x,t)$ satisfies $H(L,t) = H(L+1,t)$ for all t . This boundary condition was first stated in [2]. Fig. 1 shows two examples of the typical interface $H(x,t)$ with different initial conditions.

The mapping between the Oslo Model and the interface depinning model was first established by Paczuski and Boettcher in [2]. By means of the interface profile given by $H(x,t)$, the Oslo Model is mapped to a model of an elastic interface with a depinning quenched noise, where the interface is slowly pulled at one end and proceeds to move forward whenever the local force is positive. Later on, in [3], the map between the Oslo Model and the quenched Edwards-Wilkinson equation was established via $h(x,t)$ and its governing equation in Eq. (5), casting the Oslo Model into a simple equation of motion without the need of explicitly thresholded dynamics. In the following we assume that H follows the same scaling as h , which is implied by (10) as H and h differ only by a bounded quenched noise.

IV. AVALANCHE SIZE

The set of all possible stable configurations of the pile is composed by two subsets, namely the transient configurations and the recurrent configurations [5, 6, 31]. Recurrent configurations are those the pile can end up in with finite probability an arbitrarily long time after initialisation, transient configurations are all others. Accordingly, the set of recurrent states is the attractor subset in the space of all possible configurations. It is in this regime where the observables are statistically homogeneous and, for this reason, they are said to be at stationarity. In our numerical simulations we make sure that we initialise the pile in a recurrent configuration, randomly chosen with the correct weight, by setting $z_x = 2$ for all x , z_x^c random, and driving once before start recording the observables [7].

The avalanche size s is the number of topplings that occur between two consecutive quiescent states. In the interface picture, the avalanche size is equivalently defined as the area enclosed between two consecutive stable interface configurations,

$$s_t = \sum_{x=1}^L (H(x, t+1) - H(x, t)), \quad (11)$$

see Fig 2. Beyond a lower cutoff s_0 , the avalanche size s has a power law probability distribution up to a large scale cutoff

$$P(s; L) = a s^{-\tau} \mathcal{G}\left(\frac{s}{bL^D}\right), \quad (12)$$

where a and b are metric factors, \mathcal{G} is a scaling function, $\tau > 1$ is the avalanche size exponent and D is the avalanche dimension; L^D being the characteristic avalanche size. In the one-dimensional model, the exponents have been reported to be $\tau = 1.5556 \pm 0.0005$ and $D = 2.250 \pm 0.002$, and they have been conjectured to be the rational numbers $D = \frac{9}{4}$ and $\tau = \frac{14}{9}$ [1, 2, 4, 6]. By performing the change of variable $u = s/L^D$ we find that the moments of the avalanche size,

$$\begin{aligned} \langle s^n \rangle &= \int s^n P(s; L) ds \\ &= a b^{1+n-\tau} L^{D(1+n-\tau)} \gamma_n, \end{aligned} \quad (13)$$

where $\gamma_n = \int_0^\infty u^{n-\tau} \mathcal{G}(u) du$ is a constant, scale as $\langle s^n \rangle \propto L^{\sigma_n}$ where $\sigma_n = D(n+1-\tau)$ for $n > \tau - 1$. Once the pile is in a recurrent state, each grain that is added to the pile results, on average, in one grain coming out of the pile and, for this to happen in the case $d = 1$, on average one grain has to traverse the entire lattice resulting in an avalanche of size L . Thus, the expected value of the avalanche size is $\langle s \rangle = L$, which implies $\sigma_1 = D(2-\tau) = 1$.

In [2, 32] the mapping between the Oslo Model and the depinning model is established and the relation between the exponents is shown to be

$$D = \chi + d, \quad (14)$$

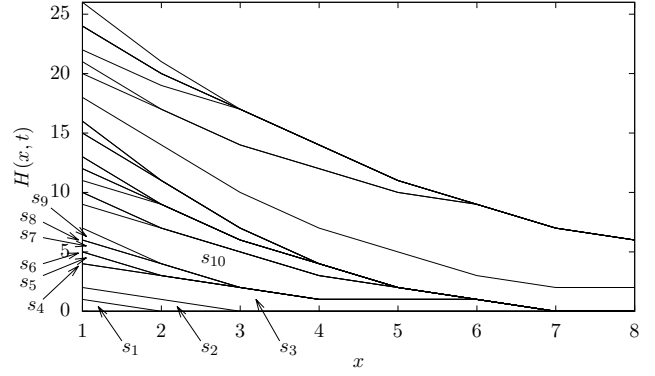


FIG. 2. Example in detail of $H(x, t)$ of a one-dimensional boundary driven pile of size $L = 8$ with initial state $z_x = 1$ and z_x^c chosen at random for all x . The series of avalanche sizes is $\{1, 2, 9, 0, 1, 0, 2, 0, 1, 11, \dots\}$, according to (11).

where χ is the roughness exponent and d is the dimension of the pile. The key argument is that the roughness exponent characterises the vertical fluctuations of the interface $H(x, t)$, which has a characteristic scale L^χ . The characteristic volume enclosed between interfaces is then $L^\chi L^d$, which in the Oslo Model is equivalent to the characteristic avalanche size L^D , hence Eq. (14).

V. MULTIPLE DRIVE AVALANCHE SIZE

The estimator \bar{s} of the first moment of the avalanche size is to be calculated in the following from a sequence of M consecutive samples s_i , Eq. (2) with $i = t+1, \dots, t+M$. Since the macroscopic timescale is measured in units of the number of grains added to the pile, M is a measure of time and drive size, and, therefore, a measure of the sample size of \bar{s} as well. We define the multiple drive avalanche size $S(t, M; L)$ as the sum of M consecutive avalanche sizes, i.e. $S(t, M; L) = \sum_{i=t+1}^{t+M} s_i$ stationary in t . By the Abelianess [7] of the Oslo Model, the total avalanche size triggered by M simultaneous charges is identical to the sum of M consecutive avalanche sizes. Since the estimate is $\bar{s} = S(t, M; L)/M$, studying fluctuations of \bar{s} as a function of sample size M is equivalent to determining how $\langle S^n(t, M; L) \rangle$ and its variance scale in M and L which is what we are going to do in the following. For simplicity, our argument is applied to $d = 1$, although it can be generalised to higher dimensions.

If the samples are taken consecutively starting at some time t , summing over the M samples is the same as considering the total area enclosed between the interfaces $H(x, t+M)$ and $H(x, t)$, Eq. (11). Thus,

$$S(t, M; L) = \sum_{x=1}^L (H(x, t+M) - H(x, t)). \quad (15)$$

Using Eqs. (7) and (10) we have

$$H(x, t) = E(t) + \frac{1}{2} \left[\eta_{x,t} + \sum_{i=1}^x i a_{i,t} + x \sum_{i=x+1}^L a_{i,t} \right], \quad (16)$$

and using Eq. (15) we see that $S(t, M; L)$ can be expressed as the sum of a deterministic term and a noise

$$S(t, M; L) = ML + \xi(t, M; L), \quad (17)$$

where $\xi(t, M; L)$ is the random variable

$$\begin{aligned} \xi(t, M; L) = & \frac{1}{2} \sum_{x=1}^L \left[\eta_{x,t+M} - \eta_{x,t} \right. \\ & + \left(x(L+1-x) + \frac{1}{2}x(x-1) \right) \\ & \left. \times (\eta_{x-1,t+M} + \eta_{x+1,t+M} - \eta_{x-1,t} - \eta_{x+1,t}) \right]. \end{aligned} \quad (18)$$

The noise $\xi(t, M; L)$ is a finite sum of bounded random variables and therefore a bounded random variable itself.

The mapping with the depinning model suggests that M , which accounts for the distance at the left boundary between two interface configurations, is to be compared with the characteristic scale of the vertical fluctuations L^χ , which is the distance at which the interfaces typically detach [5]. In the following we determine a characteristic drive size M^* and show $\langle S(t, M; L) \rangle = ML$ from the interface picture. Since the curvature of $h(x, t)$ is bounded due to Eq. (6), this feature is inherited by the interfaces $H(x, t)$ via Eq. (10) and therefore the curvature $\Delta H(x, t)$ is bounded too. From this fact and the boundary condition $H(L, t) = H(L+1, t)$ it follows that, in the quiescent state, $\partial_x H(x, t) \equiv H(x+1, t) - H(x, t)$ fluctuates about an average, i.e. $\langle \partial_x H(x, t) \rangle$ is independent of t . Hence, the average distance $\langle H(x, t_i) - H(x, t_j) \rangle$ satisfies

$$\partial_x \langle H(x, t_i) - H(x, t_j) \rangle = 0, \quad (19)$$

in all dimension (with suitable boundary conditions), for any x, t_i and t_j . Therefore the average distance between two interfaces is constant and is given by the boundary condition,

$$\langle H(x, t+M) - H(x, t) \rangle = M. \quad (20)$$

Using Eq. (15) it follows that

$$\langle S(t, M; L) \rangle = \sum_{x=1}^L \langle H(x, t+M) - H(x, t) \rangle = ML, \quad (21)$$

and therefore $D(2-\tau) = 1$ for the exponents introduced in Eq. (13). Further using Eq. (14) we have $\chi = D(\tau-1)$. Hence, the ratio of the drive size M over the distance of typical detachment L^χ (in units of drives) is

$$\frac{M}{L^\chi} = \frac{M}{L^{D(\tau-1)}}. \quad (22)$$

In the following we use $M^* = L^{D(\tau-1)}$ as the typical drive size for two interfaces to detach completely. As we show below, the moments of $S(t, M; L)$ scale differently in the regimes $M \ll M^*$ and $M \gg M^*$.

A. Short timescales (before detachment), $M \ll M^*$

Firstly, we assume that a scaling form like Eq. (12) applies to $P(S; M, L)$, the probability distribution of the avalanche size S resulting from M charges, with the additional argument $M/L^{D(\tau-1)}$,

$$P(S; M, L) = a M^\mu S^{-\tau} \mathcal{F} \left(\frac{S}{b L^D}, \frac{M}{c L^{D(\tau-1)}} \right), \quad (23)$$

where a, b and c are metric factors, \mathcal{F} is a scaling function such that if $M = 1$ then Eq. (23) is exactly Eq. (12) and μ is an additional exponent to be determined in the following. To do so we assume that $P(S; M, L)$ is invariant under simultaneous rescaling of S, L and M using the rescaling coefficient λ , so that

$$P(S; M, L) dS = P \left(\frac{S}{\lambda^D}; \frac{M}{\lambda^{D(\tau-1)}}, \frac{L}{\lambda} \right) \frac{dS}{\lambda^D} \quad (24)$$

for all λ . Using Eq. (23) it follows that $1 = \lambda^{D\tau} \lambda^{-\mu D(\tau-1)} \lambda^{-D}$ for all λ which determines μ to be unity. Integrating Eq. (23) produces the moments of S ,

$$\langle S^n(M, L) \rangle = ab^{1+n-\tau} M L^{D(1+n-\tau)} \mathcal{H}_n \left(\frac{M}{c L^{D(\tau-1)}} \right). \quad (25)$$

Choosing $M = 1$ we can infer that $\mathcal{H}_n(x) \rightarrow \gamma_n$ in the limit of small x as to recover $\langle s^n \rangle \propto L^{D(1+n-\tau)}$ from Eq. (13).

The scaling form Eq. (25) indicates that for $M \ll M^*$, the moments of S with $n > \tau - 1$ scale linearly in M . Our numerical results in Fig. 3 confirm this behaviour. This is surprising as one may expect the n th moments of sums of M avalanche sizes to scale like M^n .

B. Long timescales (after detachment), $M \gg M^*$

The correlations between detached interfaces are not so strongly dominated by their vertical fluctuations and roughness but rather by the global features of the interface. We derive the moments $\langle S^n(M; L) \rangle$ from Eq. (17),

$$\begin{aligned} \langle S^n(M; L) \rangle = & (ML)^n + n(ML)^{n-1} \langle \xi \rangle \\ & + \binom{n}{2} (ML)^{n-2} \langle \xi^2 \rangle + \dots + \langle \xi^n \rangle, \end{aligned} \quad (26)$$

and proceed by characterising $\langle \xi^n \rangle$.

From Eq. (18) we deduce that $\langle \xi \rangle = 0$: since ξ is defined as the difference of two quantities at quiescence, one at t and one at $t+M$, due to stationarity the expectation of each of these quantities is the same and, therefore, they cancel each other when calculating the expectation $\langle \xi \rangle$. Moreover, assuming that the n -point correlation of H displays standard gap-scaling, e.g. $\langle H(x_1, t_1) H(x_2, t_2) H(x_3, t_3) \rangle \propto L^{3\chi} \mathcal{C}_3(\dots)$, Eq. (A6), it follows that $\langle \xi^n \rangle = L^{nD} \Xi_n(M/L^{D(\tau-1)})$, as shown for $n = 1$ in Eq. (A7). Writing $ML = L^D (M/L^{D(\tau-1)})$ by

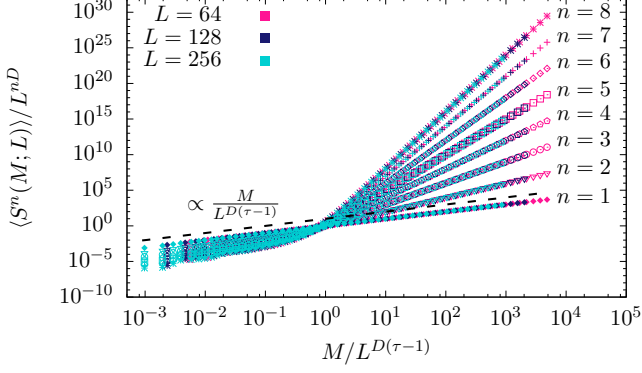


FIG. 3. Data collapse of the moments $\langle S^n(M; L) \rangle$ according to Eq. (27) (or (25)) with $n \in \{1, 2, 3, 4, 5, 6, 7, 8\}$ as a function of $M/L^{D(\tau-1)}$ for the system sizes $L \in \{64, 128, 256, 512\}$. The black dashed line shows a line with slope 1 to emphasise the linearity of $\langle s^n \rangle$ in small M , Eq. (25).

using $D(2-\tau) = 1$ it follows that every term in (26) is of the form $L^{nD} f_n(M/L^{D(\tau-1)})$ with some function $f_n(x)$ incorporating the scaling function $\Xi_n(x)$ of the noise and other coefficients, so that finally

$$\langle S^n(M; L) \rangle = L^{nD} \mathcal{K}_n \left(\frac{M}{L^{D(\tau-1)}} \right) \quad (27)$$

Fig. 3 shows a collapse of numerical data according to Eq. (27). The scaling of $\langle S^n \rangle$ in large M follows from Eq. (26), which is dominated by $(ML)^n$, given that ξ is asymptotically independent of (large) M . This implies that $\mathcal{K}_n(x) \propto x^n$ in large x , as $L^{nD} (M/L^{D(\tau-1)})^n = (ML)^n$. Further Eq. (27) is in line with Eq. (25) as $x\mathcal{H}_n(x) = \mathcal{K}_n(x)$.

VI. DISCUSSION

In the following, we characterise the fluctuations of the estimate of the mean avalanche size $\bar{s} = \frac{1}{M} \sum_{i=1}^M s_i$. The scaling form of $\sigma^2(\bar{s}) = \sigma^2(S(M; L))/M^2$ is derived as

$$\sigma^2(\bar{s}) = L^2 \mathcal{D} \left(\frac{M}{L^{D(\tau-1)}} \right) \quad (28)$$

using $\langle S^2(M; L) \rangle \propto ML^{D(3-\tau)}$ from Eq. (25), $D(2-\tau) = 1$ and multiplying by the argument of the scaling function $\mathcal{D}(M/M^*)$ once.

In order to derive the scaling form of $\mathcal{D}(x)$ in each regime we use Eqs. (25) and (26). For $M \ll M^*$, it follows that $\sigma^2(\bar{s}) \propto M^{-1}$. For $M \gg M^*$, it follows $\sigma^2(S(M; L)) = \sigma^2(\xi) \propto KL^{2D}$ and, therefore, $\sigma^2(\bar{s}) = \sigma^2(\xi)/M^2 \propto M^{-2}$. In summary, the scaling function $\mathcal{D}(x)$ has the form

$$\mathcal{D}(x) \propto \begin{cases} x^{-1} & \text{if } x \ll 1, \\ x^{-2} & \text{if } x \gg 1, \end{cases} \quad (29)$$

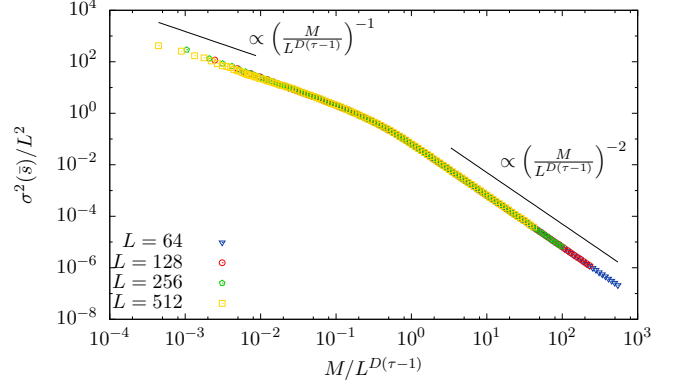


FIG. 4. Data collapse of $\sigma^2(\bar{s})$ as a function of $M/L^{D(\tau-1)}$ according to Eq. (28). The variance is compared to plain power law, shown as straight lines, in the two regimes $M \ll L^{D(\tau-1)}$ and $M \gg L^{D(\tau-1)}$. The values of M are approximately exponentially spaced and lie in the range $[1, 10^5] \in \mathbb{N}$. For each M , the variance $\sigma^2(\bar{s}(M))$ has been computed from a sample set of $2 \cdot 10^4$ estimates of $\langle s \rangle$.

indicating a crossover between the two scaling regimes. Moreover, in the second $M \gg M^* = L^{D(\tau-1)}$ regime the avalanche size s is hyperuniform with exponent $\lambda = 2$ [23–25]. Fig. 4 shows a data collapse of $\sigma^2(\bar{s})$ for a range of M and different L .

For $M \ll M^*$, the moments of S scale linearly in M , that is $\langle S^n(M; L) \rangle \propto M$, which implies that the fluctuations of the estimate \bar{s} have the scaling form $\sigma^2(\bar{s}) \propto M^{-1}$ as if \bar{s} was based on M independent samples. After detachment, $M \gg M^*$, we find that the conservation of the area ML enclosed by two interfaces causes the variance of \bar{s} to vanish as quickly as M^{-2} , which is the fingerprint of enhanced hyperuniformity [27]. Hyperuniformity for $M \gg M^*$ implies, counterintuitively, that a regularity in s emerges in the long timescales from the correlations between avalanches in the short timescales.

As for the computational aspect of the Oslo Model, the rapid convergence of \bar{s} above means that for a fixed sample size M , more precise statistics are obtained when the samples are taken sequentially rather than independently. Contrary to what one may expect, the intricate correlations between avalanches can be used to an advantage in numerical simulations, providing us with a recipe for higher precision as well as for reducing the computational time.

A. Higher moments of s

The estimators of higher moments are $\bar{s}^n(M) = \frac{1}{M} \sum_{i=1}^M s_i^n$. Because there is no conservation law such as the area conservation discussed above, we cannot derive hyperuniformity for higher moments analytically. Despite the rate of convergence of the estimates being proportional to M^{-1} , our numerical simulations show

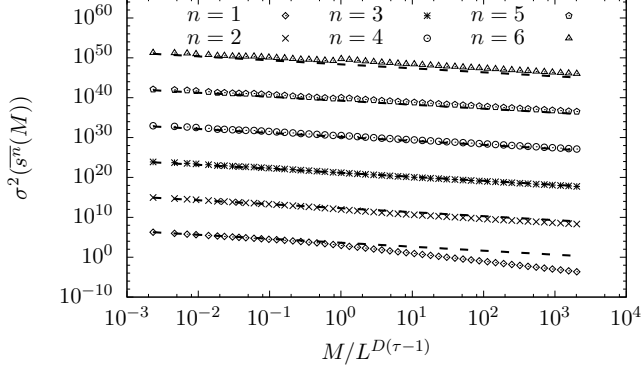


FIG. 5. Variance $\sigma^2(\bar{s}^n(M))$ as a function of $M/L^{D(\tau-1)}$ for the system size $L = 128$. The dashed lines indicate the variance of the estimator \bar{s}^n if the M samples were independent, i.e. $\sigma^2(\bar{s}^n(1))/M$. Although only the first moment is hyperuniform, with $\sigma^2(\bar{s})$ decaying as fast as M^{-2} , in all cases the fluctuations are suppressed when consecutive samples are taken, $\sigma^2(\bar{s}^n(M)) < \sigma^2(\bar{s}^n(1))/M$.

that the amplitude of the variance at large M is smaller than for independent samples, that is $\sigma^2(\bar{s}^n(M)) < \sigma^2(\bar{s}^n(1))/M$. This implies that for the higher moments there still is an advantage in sampling sequentially than independently, similar to the self-averaging of spatially extended observables [33]. In Fig. 5 we compare the variance of the estimates $\bar{s}^n(M)$ obtained by sequential sampling to the variance obtained for independent sampling, which, from the Central Limit Theorem [18], equals $\sigma^2(\bar{s}^n(1))/M$.

B. Uniform drive on the bulk

In [5, 34] the authors have studied the one-dimensional bulk driven Oslo Model on a lattice with open boundaries. To derive the scaling of $\sigma^2(\bar{s})$ from similar considerations as above, we note that the boundary conditions are now $h(0, t) = h(L+1, t) = 0$ for all t and the equation of motion has an additional source term $E(x, t) = \sum_{j=1}^t \theta(t-j) \delta_{x, x_j}$, where $\theta(t)$ is the Heaviside step function, $\delta_{x, y}$ is the Kronecker delta and $x_j \in \{1, \dots, L\}$ for $j = 1, \dots, t$ are uniformly distributed driving sites. The source $E(x, t)$ accounts for the number of external grains that have been dropped at x up to time t . The equation of motion now reads

$$h(x, t + \delta t) - h(x, t) = E(x, t) + \frac{1}{2} [h(x-1, t) - 2h(x, t) + h(x+1, t) + \eta_{x-1, t} + \eta_{x+1, t}], \quad (30)$$

which, at quiescence, has the solution

$$h(x, t) = \left(1 - \frac{x}{L+1}\right) \sum_{i=1}^{x-1} i b_{i, t} + \frac{x}{L+1} \sum_{i=x}^L (L+1-i) b_{i, t}, \quad (31)$$

where $b_{x, t} = -\Delta h(x, t)|_{t \in \mathbb{Z}} = 2E(x, t) + \eta_{x-1, t} + \eta_{x+1, t}$. Fig. 5(a) shows an example of the typical interface $H(x, t)$ for a range of t . Using Eqs. (10), (15) and (31), the multiple drive avalanche size can be derived to be

$$S(M; L) = \frac{1}{2} \sum_{x=1}^L \left[\eta_{x, t+M} - \eta_{x, t} + \frac{x}{2} (L+1-x) (b_{x, t+M} - b_{x, t}) \right] = \Lambda(M; L) + \xi'(M; L), \quad (32)$$

where the random variable

$$\Lambda(M; L) = \frac{1}{2} \sum_{x=1}^L x(L+1-x) (E(x, t+M) - E(x, t)) \quad (33)$$

is due to the drive and

$$\xi'(M; L) = \frac{1}{2} \sum_{x=1}^L \left[\eta_{x, t+M} - \eta_{x, t} + \frac{x}{2} (L+1-x) (\eta_{x-1, t+M} + \eta_{x+1, t+M} - \eta_{x-1, t} - \eta_{x+1, t}) \right] \quad (34)$$

is the noise term. The key difference between Eq. (34) and the corresponding noise Eq. (18) for the boundary-driven Oslo Model considered above are the boundary conditions applied to h . From Eq. (32) we have that $\sigma^2(S(M; L)) = \sigma^2(\Lambda) + \sigma^2(\xi') + \text{Cov}(\Lambda, \xi')$. The variance of $\Lambda(M; L)$ can be calculated using the fact that the vector of random variables $\mathbf{E}(t+M) - \mathbf{E}(t)$ has a multinomial distribution independent of t with probabilities $p_x = 1/L$ for all x and M trials, giving

$$\sigma^2(\Lambda(M; L)) = \frac{1}{720} M (L^4 - 5L^2 + 4). \quad (35)$$

Following the same argument as in Sect. V, since $\xi'(M; L)$ is bounded, its variance does not scale in M . Finally, due to the nature of Λ and ξ' , it follows that $\text{Cov}(\Lambda, \xi')$ is subleading in M compared to $\sigma^2(\Lambda)$ as $M \rightarrow \infty$. Therefore, the variance $\sigma^2(S(M; L)) \propto ML^4$ and this implies $\sigma^2(\bar{s}) \propto M^{-1}L^4$, implying that the avalanche size of the uniformly driven Oslo Model does not display hyperuniformity.

Our numerical results, Fig. 5(b), show that the variance follows the asymptotic scaling form

$$\sigma^2(\bar{s}) = L^{3.5} \tilde{\mathcal{D}} \left(\frac{M}{L^{0.5}} \right), \quad (36)$$

with $\tilde{\mathcal{D}}(x) \propto x^{-1}$ as $x \rightarrow \infty$. That is, asymptotically, $\sigma^2(\bar{s}) \propto M^{-1}L^4$. In fact, at large M the scaling in Eq. (36) is solely due to Eq. (35) as $\sigma^2(\bar{s})$ is dominated entirely by $\sigma^2(\Lambda)/M^2$. The interfaces detach dominantly due to the noise in the driving rather than the fluctuations of the interface.

If the driving position x is fixed, then $\Lambda(M; L) = \frac{1}{2} x(L+1-x)M$ becomes deterministic so that $\sigma^2(\Lambda) = 0$

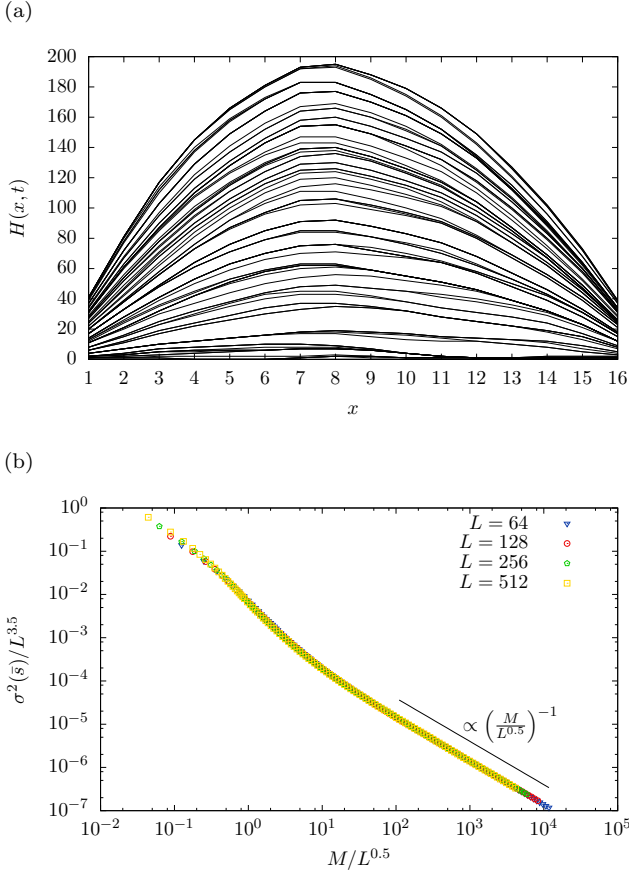


FIG. 6. One-dimensional bulk driven Oslo Model with open boundary conditions. (a) Typical interface configurations of topplings $H(x, t)$ in a system of size $L = 16$ with total drive size $M = 90$ (for illustration purposes, the initial condition is $z_x = 1$ for all x); (b) The scaling of the variance $\sigma^2(\bar{s})$ is asymptotically proportional to $M^{-1}L^4$ (measurements have been taken starting from recurrent configurations).

and the results for the boundary-driven Oslo Model generalise to the Oslo Model driven at a fixed (bulk) site. Therefore, its avalanche size is hyperuniform on long timescales regardless of the driving position x and the boundary conditions. In particular, if the drive is located at the boundary $x = 1$ then $\Lambda(M; L) = \frac{1}{2}LM$, where the difference in the $1/2$ factor with Eq. (17) is due to the different boundary conditions.

C. Two-dimensional Oslo Model

We also study the fluctuations in the avalanche size in the two following scenarios on a square lattice: (a) two open and two closed boundaries with the drive located at the intersection of two open boundaries (corner drive) and (b) four open boundaries and uniformly distributed drive on the lattice (bulk drive). These two scenarios resemble the one-dimensional studied cases studied above. Our numerical results for scenario (a) are shown in Fig.

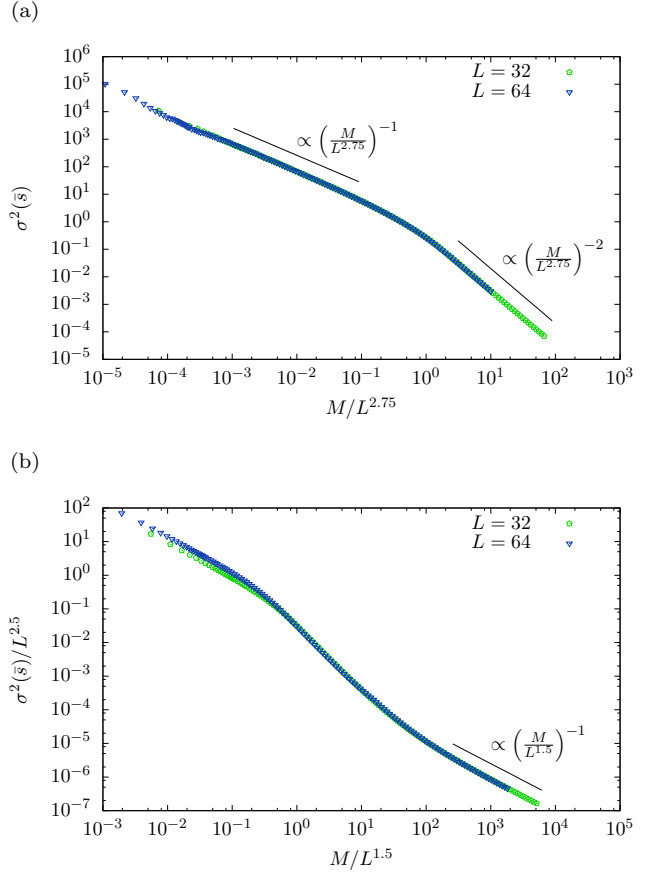


FIG. 7. Two-dimensional Oslo Model with different drive and boundary conditions. In all cases, the pile is initialised in a recurrent configuration. We show the scaling of $\sigma^2(\bar{s})$ for the cases (a) two open and two closed boundaries with the drive located at the intersection of the two open boundaries (see Fig. 4) and (b) four open boundaries with drive uniformly distributed in the bulk (see Fig. 6). Similarly to the one-dimensional cases, in (a) the fluctuations $\sigma^2(\bar{s})$ have two scaling regimes, displaying hyperuniformity for $M \gg M/L^{2.75}$, and in (b) $\sigma^2(\bar{s})$ is asymptotically proportional to $M^{-1}L^4$.

6(a). The variance has the scaling form

$$\sigma^2(\bar{s}) = \mathcal{D} \left(\frac{M}{L^{2.75}} \right), \quad (37)$$

with $\mathcal{D}(x)$ defined in Eq. (29). The exponent 2.75 is in fact the avalanche dimension $D = 2.75 \pm 0.01$ [5, 34, 35], which enters into the characteristic number of driving steps, $M^* \propto L^{D(\tau-1)}$. Since the average avalanche size diverges only logarithmically, $\sigma_1 = D(2 - \tau) = 0$, in the case of corner drive with boundary conditions as described above, it follows that $\tau = 2$ hence $D(\tau - 1) = D$. Further, the second moment of S scales like $ML^{D(3-\tau)} = ML^D$, Eq. (25), so that

$$\sigma^2(\bar{s}) \propto \frac{1}{M^2} \langle S^2(M; L) \rangle = \frac{1}{M} L^D \mathcal{H}_2 \left(\frac{M}{L^D} \right) = \mathcal{D} \left(\frac{M}{L^D} \right). \quad (38)$$

TABLE I. Summary of our results for each of the studied scenarios: the exponent σ_1 , the crossover point M^* of $\sigma^2(\bar{s})$ and its scaling behaviour for large M .

	Drive	σ_1	M^*	Large M behaviour
1D	corner	1	$L^{D(\tau-1)} = L^\chi$	$\sim M^{-2}$, hyperuniform
	uniform bulk	2	$L^{1/2}$	$\sim M^{-1}$, Poisson-like
2D	corner	0	$L^{D(\tau-1)} = L^{\chi+2}$	$\sim M^{-2}$, hyperuniform
	uniform bulk	2	$L^{3/2}$	$\sim M^{-1}$, Poisson-like

In scenario (b), Fig. 6(b), we find numerically that the variance has the scaling form

$$\sigma^2(\bar{s}) = L^{2.5} \tilde{\mathcal{D}} \left(\frac{M}{L^{1.5}} \right), \quad (39)$$

following the same scaling as the one-dimensional bulk driven Oslo Model, $\sigma^2(\bar{s}) \propto M^{-1} L^4$ in large M , Eq. (25), as, again, fluctuations of \bar{s} are dominated by the driving rather than the interface roughness.

Our results are summarised in Tab. I. Depending on the driving, the scaling of $\sigma^2(\bar{s})$ in M is dominated either by the variance of the noise (i.e. the fluctuations of the interface) or the variance of the deterministic term (essentially the driving itself) in S , Eqs. (17) or (32). In case of the former, $D = \chi + d$ is restored by all moments scaling linearly in M for $M \ll L^{D(\tau-1)}$, while hyperuniformity is found for $M \gg L^{D(\tau-1)}$. In case of the latter the randomness of the drive means that asymptotically $\sigma^2(\bar{s}) \propto M^{-1}$. [36]

When the drive is located to one position, it is well known that if we sample independently then $\bar{s} = (\sum_{i=t+1}^{t+M} s_i) / M$ shows the usual variance of an averaged random variable, $\sigma^2(\bar{s}) = \sigma^2(s) / M$ [18]. Conversely, our results imply that if we sample sequentially, then $\bar{s} = L + \xi / M$ and the variance is determined only by that of ξ / M , yielding $\sigma^2(\bar{s}) = \langle \xi^2 \rangle / M^2$.

In conclusion, in this paper we have proven that the fluctuations of the avalanche size of the Oslo Model with external drive located in one fixed position displays a crossover from Poisson-like behaviour at short timescales to hyperuniform behaviour at long timescales. Therefore, the time series of avalanches is an example of a disordered hyperuniform system. The quantity that is conserved on the long timescale is the area between interface configurations in the interface picture. On short timescales, fluctuations are not much constrained by the conserved area and weaker correlations between consecutive interface configurations produce Poisson-like scaling.

We have found that the conservation of the area is due to (a) the existence of an interface picture and (b) the boundedness of the curvature of the interfaces. Condition (a) is not sufficient, as is shown for the bulk-driven Oslo Model. It remains an open question whether hyperuniformity implies the existence of an interface picture. Finding hyperuniformity in other models will help to understand its role in the context of Self-Organised

Criticality.

Appendix A: Correlation function of the interfaces

As discussed in Sect. IV, the scaling form of $P(s; L)$ in Eq. (12) gives the scaling in L of the moments of the avalanche size, which is $\langle s^n \rangle \propto L^{\sigma_n}$ with $\sigma_n = D(n+1-\tau)$. However, as we show here, a scaling form like Eq. (12) is not enough to characterise the moments of the multiple drive avalanche size $S(M; L)$ and that Eq. (23) is needed instead.

Using the correlation function of the interfaces, we show that assuming the scaling form Eq. (12) for $P(S, M; L)$ leads to a contradiction and therefore it needs to be amended by introducing an additional argument that relates M and L .

To compute the variance of S , we have from Eq. (15)

$$\langle S \rangle^2 = \iint \langle H(x, t+M) - H(x, t) \rangle \times \langle H(x', t+M) - H(x', t) \rangle d^d x d^d x', \quad (A1)$$

and

$$\langle S^2 \rangle = \iint \langle (H(x, t+M) - H(x, t)) \times (H(x', t+M) - H(x', t)) \rangle d^d x d^d x', \quad (A2)$$

which can be calculated on the basis of the correlation function

$$c(x, x', t, t') = \langle H(x, t) H(x', t') \rangle - \langle H(x, t) \rangle \langle H(x', t') \rangle = c(x', x, t', t). \quad (A3)$$

The variance, then, reads

$$\begin{aligned} \sigma^2(S) &= \langle S^2 \rangle - \langle S \rangle^2 \\ &= \iint (c(x, x', t+M, t+M) - c(x, x', t+M, t)) d^d x d^d x' \\ &\quad + \iint (c(x, x', t, t) - c(x, x', t, t+M)) d^d x d^d x' \\ &= 2 \iint (c(x, x', t+M, t+M) - c(x, x', t+M, t)) d^d x d^d x', \end{aligned} \quad (A4)$$

where the last equality is due to the stationarity of $c(x, x', t+M, t+M) = c(x, x', t, t)$, swapping of dummy variables and the symmetry (A3).

The usual (translationally invariant) scaling form of the correlation function [37, 38] is

$$c(x, x', t, t') = a |x - x'|^{2\chi} \mathcal{C} \left(\frac{t - t'}{b |x - x'|^z} \right), \quad (A5)$$

where \mathcal{C} is a scaling function, a and b are metric factors, χ is the roughness exponent as introduced in Eq. (14) and z is the dynamical exponent which gives rise to the characteristic avalanche duration $\sim L^z$ in units of microscopic time steps. On that scale, the time span $t - t' = M$

considered here is very large for any M , as any avalanche must have completed in order to obtain its size. Increasing $t - t'$ further makes no difference to $\sigma^2(S)$ and we conclude that $c(x, x', t, t') \sim a|x - x'|^{2\chi}$. Integrating according to (A4) then produces $\sigma^2(S) \sim L^{2d+2\chi}$, irrespective of M . Using (14) it follows that $\sigma_2 = 2D$, as $\sigma^2(S)$ is dominated in L by $\langle S^2 \rangle \gg \langle S \rangle^2$ for $M = 1$, in contradiction to $\sigma_2 = \sigma_1 + D$, from Eq. (13), unless $\sigma_1 = D$ and thus $\tau = 1$, which does not apply for any of the boundary conditions considered.

To cure this contradiction, we need to consider the scaling of correlations on the macroscopic timescale. Its characteristic value M^* is given by the number of avalanches needed to make the interface configuration uncorrelated. Given Neumann and Dirichlet boundary conditions at opposing ends, the total volume between detached interfaces is of order $L^d L^\chi$, filled in $M^* \propto L^{\chi+d}/\langle s \rangle \propto L^{\chi+d+\sigma_1}$ driving steps. Amending the scaling function in (A5) accordingly

$$c(x, x', t, t') = a|x - x'|^{2\chi} \mathcal{C} \left(\frac{t - t'}{b|x - x'|^z}, \frac{t - t'}{cL^{\chi+d+\sigma_1}} \right), \quad (\text{A6})$$

gives with $\chi + d = D$, Eq. (14),

$$\sigma^2(S) = aL^{2D} \mathcal{D} \left(\frac{M}{cL^{D-\sigma_1}} \right). \quad (\text{A7})$$

Demanding further that $\sigma^2(S) \propto L^{D+\sigma_1}$ in large L implies that $\mathcal{D}(x) \propto x$ for small arguments, so that

$$\sigma^2(S) = aML^{D(3-\tau)} \tilde{\mathcal{D}} \left(\frac{M}{cL^{D(\tau-1)}} \right) \quad (\text{A8})$$

using $D + \sigma_1 = D(3 - \tau)$ and $D - \sigma_1 = D(\tau - 1)$. The scaling function $\tilde{\mathcal{D}}(x)$ is convergent in small arguments and remarkably, $\sigma^2(S)$ is linear in $M \ll cL^{D(\tau-1)}$. Further, we expect that the scaling function of the avalanche size distribution $P(S; M, L)$ to acquire the additional argument $M/(cL^{D(\tau-1)})$, for the same reasons as the scaling functions \mathcal{C} and \mathcal{D} above did.

ACKNOWLEDGMENTS

We would like to thank Saoirse Amarteifio for helpful discussions about the BTW model, Andy Thomas for invaluable computing support and Benjamin Walter for pointing out the etymology of the words *hyperuniform* and *superhomogeneous*.

-
- [1] K. Christensen, Á. Corral, V. Frette, J. Feder, and T. Jøssang, Phys. Rev. Lett. **77**, 107 (1996).
 - [2] M. Paczuski and S. Boettcher, Phys. Rev. Lett. **77**, 111 (1996).
 - [3] G. Pruessner, Phys. Rev. E **67**, 030301 (2003).
 - [4] P. Grassberger, D. Dhar, and P. K. Mohanty, Phys. Rev. E **94**, 042314 (2016).
 - [5] G. Pruessner, *Self-Organised Criticality: Theory, Models and Characterisation* (Cambridge University Press, 2012).
 - [6] K. Christensen and N. R. Moloney, *Complexity and Criticality*, Vol. 1 (Imperial College Press, 2005).
 - [7] D. Dhar, Physica A **340**, 535 (2004).
 - [8] M. Najafi, S. Moghimi-Araghi, and S. Rouhani, Phys. Rev. E **85**, 051104 (2012).
 - [9] B. Cerruti and E. Vives, Phys. Rev. E **80**, 011105 (2009).
 - [10] J. Davidsen and M. Paczuski, Phys. Rev. E **66**, 050101 (2002).
 - [11] H. Leschhorn and L.-H. Tang, Phys. Rev. E **49**, 1238 (1994).
 - [12] M. Benayoun, J. D. Cowan, W. van Drongelen, and E. Wallace, PLoS Comput Biol **6**, e1000846 (2010).
 - [13] F. Lombardi, H. J. Herrmann, D. Plenz, and L. de Arcangelis, Sci. Rep. **6** (2016).
 - [14] Á. Corral, Tectonophysics **424**, 177 (2006).
 - [15] T. Mori and H. Kawamura, Phys. Rev. Lett. **94**, 058501 (2005).
 - [16] O. Ramos, E. Altshuler, and K. Måløy, Phys. Rev. Lett. **102**, 078701 (2009).
 - [17] S. Janićević, L. Laurson, K. J. Måløy, S. Santucci, and M. J. Alava, Phys. Rev. Lett. **117**, 230601 (2016).
 - [18] N. G. Van Kampen, *Stochastic Processes in Physics and Chemistry*, Vol. 1 (Elsevier, 1992).
 - [19] A. Papoulis, *Probability, Random Variables, and Stochastic Processes* (McGraw-Hill, 1965).
 - [20] C. Gardiner, Applied Optics **25**, 3145 (1986).
 - [21] I. I. Gikhman and A. V. Skorokhod, *The Theory of Stochastic Processes I* (Springer, 2015).
 - [22] P. Welinder, G. Pruessner, and K. Christensen, New J. Phys. **9**, 149 (2007).
 - [23] S. Torquato and F. H. Stillinger, Phys. Rev. E **68**, 041113 (2003).
 - [24] D. Hexner and D. Levine, Phys. Rev. Lett. **118**, 020601 (2017).
 - [25] A. Gabrielli, M. Joyce, and F. Sylos Labini, Phys. Rev. D **65**, 083523 (2002).
 - [26] C. E. Zachary and S. Torquato, J. Stat. Mech. **2009**, P12015 (2009).
 - [27] D. Hexner, P. M. Chaikin, and D. Levine, Proc. Natl. Acad. Sci. USA.
 - [28] L. Berthier, P. Chaudhuri, C. Coulais, O. Dauchot, and P. Sollich, Phys. Rev. Lett. **106**, 120601 (2011).
 - [29] L. S. Froufe-Pérez, M. Engel, P. F. Damasceno, N. Muller, J. Haberkorn, S. C. Glotzer, and F. Scheffold, Phys. Rev. Lett. **117**, 053902 (2016).
 - [30] S. Brandt, *Data analysis* (Springer, 1999).
 - [31] A. Chua and K. Christensen, (2002), arXiv:cond-mat/0203260.
 - [32] M. Paczuski, S. Maslov, and P. Bak, Phys. Rev. E **53**, 414 (1996).

- [33] A. M. Ferrenberg, D. P. Landau, and K. Binder, J. Stat. Phys. **63**, 867 (1991).
- [34] J. A. Bonachela and M. A. Muñoz, Phys. Rev. E **78**, 041102 (2008).
- [35] S. Lübeck, Phys. Rev. E **61**, 204 (2000).
- [36] We have also studied the fluctuations of the avalanche size in the two-dimensional BTW model and the one-dimensional Manna model and, although there is a certain amount of suppression of fluctuations, neither of these models strictly show hyperuniform behaviour.
- [37] J. Krug, Adv. Phys. **46**, 139 (1997).
- [38] A.-L. Barabási and H. E. Stanley, *Fractal Concepts in Surface Growth* (Cambridge University Press, 1995).